Improving Compact Short Backfire Antenna Gain and Cross-Polarization Using Choke and Ring Cavity Loading

Amirbahador Mansoori, *Student Member, IEEE*, Dustin Isleifson, *Senior Member, IEEE*, and Lotfollah Shafai, *Life Fellow, IEEE*

***Abstract*— We present two designs that improve the gain and cross-polarization performance of the waveguide-fed short backfire (SBF) antenna by introducing a choke (SBF-2) and by loading the cavity with a metallic ring feature (SBF-2-Ring). A series of parametric simulation studies on antenna dimensions provides information on how to improve the antenna gain and cross-polarization performance while simultaneously extending the impedance bandwidth. For SBF-2, the peak gain was 16.6 dBi, the minimum cross-polarization ratio was −23.8 dB, and the maximum impedance bandwidth was 27.3%, with a gain bandwidth of 19.2%. For SBF-2-Ring, the peak gain was 15.8 dBi, the minimum cross-polarization ratio was −29.1 dB, and the maximum impedance bandwidth was 43.5%, with a gain bandwidth of 31.8%. The concepts were verified by designing, fabricating, and testing two prototypes in the microwave C-band. Excellent agreement between simulation and measurement was achieved. The measured gain for SBF-2-Ring was >14 dBi for 4.7–6.2 GHz and the worst case cross polarization in the diagonal plane was <−22 dB for 5.3–5.8 GHz. Cross-polarization in the principal planes has significantly greater bandwidth and the worst case analysis is presented to give limitations on the performance.**

***Index Terms*— Cavity-backed antennas, microwave antennas, short backfire (SBF) antenna.**

I. Introduction

THE short backfire (SBF) antenna is an established antenna design that is used in medium-gain applications where a compact structure is desired. The first designs were reported in publications by Ehrenspeck [1], [2]. Since then, prototypes with varying feed mechanisms and design optimizations have been presented in the literature [3]–[9]. The directional aspects of the antenna make it a good candidate for point-to-point communications, remote sensing, and array feeds for reflector antennas. SBF designs have been reported in the low end of the microwave spectrum (e.g., S-band), midrange as Wi-Fi antennas, X-band antennas, and even up to millimeter-wave designs [10]–[12]. The early designs were fundamentally narrowband, and therefore, research has been conducted to extend the bandwidth of operation [6], [13]. The designs scale with frequency and can be adapted to a variety of functions [14].

Recently, antennas and radiating systems have been mounted on unmanned aerial vehicles (UAVs), with applications ranging from remote sensing to search and rescue operations. Such antennas need to be compact, low profile, low mass, and highly efficient. The SBF is a strong candidate since it can be designed and fabricated to meet these needs.

Many contemporary remote sensing systems operate in the microwave C-band. For example, Radarsat-2, the Radarsat Constellation Mission (RCM), and Sentinel 1A/B operate in the C-band. Operations range from marine environmental monitoring to improving agricultural practices, all for the benefit of the world's population. Consequently, we seek to advance the design of antennas in the C-band to provide new options and possibilities for future remote sensing systems.

The overarching objective of this article is to develop and verify SBF designs that meet the operation specifications of a C-band remote sensing system. To do this, we address the following three objectives. First, the antenna design must meet several specific physical requirements, namely, low profile, low mass, and able to be constructed of stable materials that will handle space requirements. Second, the SBF must meet the desired antenna performance that is required for a radar or passive microwave sensor. These requirements are described in Section II. Third, the antenna must be relatively simple to construct and assemble. In this design, we are aiming for a prototype with a low number of parts.

In Section II, we present the design concepts, including a discussion of several candidate prototypes. In Section III, we provide measurement results from two fabricated devices that were used to verify the concepts. Section IV gives a conclusion and recommendations for next steps in the design flow.

II. Design Concepts

The conventional SBF design requires a feed element (e.g., dipole) or a waveguide feed. In our design, we used standard waveguide components that would be easily assembled into our antenna prototypes. All designs in this article used WR159

Manuscript received 2 August 2021; revised 10 January 2022; accepted 8 February 2022. Date of publication 28 March 2022; date of current version 26 July 2022. This work was supported in part by the Natural Science and Engineering Research Council of Canada (NSERC) Discovery Grant Program. *(Corresponding author: Dustin Isleifson.)*

The authors are with the Department of Electrical and Computer Engineering, University of Manitoba, Winnipeg, MB R3T 5V6, Canada (e-mail: mansoora@myumanitoba.ca; dustin.isleifson@umanitoba.ca; lot.shafai@umanitoba.ca).

Color versions of one or more figures in this article are available at https://doi.org/10.1109/TAP.2022.3161463.

Digital Object Identifier 10.1109/TAP.2022.3161463

TABLE I
ANTENNA DESIGN SPECIFICATIONS

Design Specification	Metric
Realized Gain	>14 dBi
Impedance bandwidth	500 MHz
Primary Operating Frequency	5.5 GHz
Cross-Polarization Ratio	<-22 dB
Mass	<500 g

(dimensions a = 40.386 mm and b = 20.193 mm). We selected a waveguide feed partly based on simplicity in fabrication and partly based on the greater power handling capabilities. We encountered many design tradeoffs in our development, such as configurations with reduced gain with the benefit of wide impedance bandwidth. These aspects are discussed in the presented prototypes of this section.

For our design, we established several performance metrics that were based on design requirements from existing C-band remote sensing systems and from comparison with existing designs in the literature. These are summarized in Table I. In this article, all reported wavelength scales are given with respect to 5.5 GHz in free space (i.e., $\lambda = 0.05454$ m), as this is our primary operation frequency. All simulations were performed using Ansoft HFSS.

Typically, we report on the impedance bandwidth of the antenna. However, this is not the only metric of importance. The gain bandwidth (where gain G $\geq$ Gmax $-$ 3 dBi, where Gmax is the maximum (peak) gain within the gain bandwidth) and the cross-polarization bandwidth are defining metrics for the antenna operation. In many designs (including the ones presented here), the bandwidth is less than the impedance bandwidth and is the true operating limitation of the antenna.

Furthermore, in this article, we emphasize the worst case cross polarization as a limiting performance metric. In many manuscripts, authors will often refer to the cross-polarization levels in the principal planes ($\varphi = 0°$ and 90°), where the cross polarization is theoretically zero. Measurement results in these planes are often indicative of the limitations of the measurement accuracy. We have presented cross-polarization results in the principal planes for reference and direct comparison with other works in the literature, but also present the worst case cross polarization (in this design, $\varphi = 46°$).

A. SBF-1 Design

We developed several prototype designs. The first design, SBF-1, which was based on the conventional waveguide-fed SBF, gave reasonable performance with respect to our design specifications. In our design process, we started with a smooth main reflector to establish a benchmark for a C-band SBF design [15]. The geometry of the SBF-1 design is shown in Fig. 1. By reviewing our simulation results, we established that for all designs with a main reflector diameter (D_m) that was less than 1.8λ, the realized gain did not exceed 11 dBi. This meant that the benefit of using an SBF structure would be negated, as a similar gain could be achieved through the use of a simple open-ended waveguide. For our SBF-1 design, the highest realized gain was 14.88 dBi, and this was found for $D_m = 2.2\lambda$. Consequently, our remaining designs in this

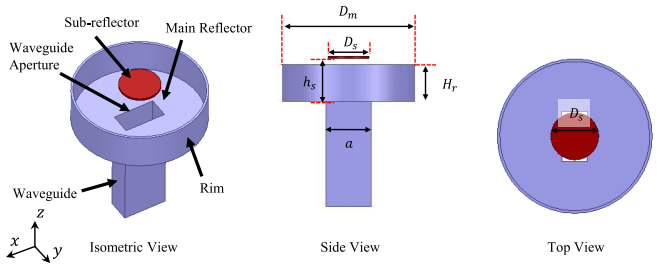

Fig. 1. SBF-1 geometry. Main reflector has a flat bottom.

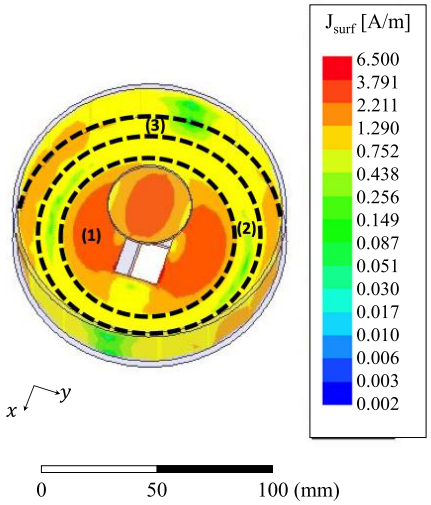

Fig. 2. SBF-1 surface current distribution.

article used $D_m = 2.2\lambda$. The rim height was set to 0.6λ, based on recommendations in the published literature [16]. The best configuration that we could derive had an impedance bandwidth of 1.45 GHz (26.4%). When we evaluated the cross polarization, we found that while the levels in the principal planes (i.e., $\varphi = 0°$ and $\varphi = 90°$) easily met the specification, the peak cross polarization (which was in $\varphi = 46°$) was significantly worse, giving a cross-polarization ratio of only -16.5 dB.

The surface current distribution of SBF-1 at 5.5 GHz is shown in Fig. 2. Current maxima are observed near the wide edge of the waveguide aperture (region 1) and on the subreflector. Region (2) has a relatively low surface current, and in region (3), current maxima are seen near the edges of the main reflector aligning with the y-axis. The aperture field distribution for SBF-1 at 5.5 GHz (on a fictitious circular surface with a diameter of 6λ, located 1λ above the subreflector, as shown in Fig. 3) exhibits a nonuniform characteristic, with large peak electric field magnitudes in the areas along the x-axis and immediately above the waveguide opening.

We investigated ways to modify the surface current distribution in order to simultaneously improve the impedance bandwidth and the gain. The approach considers a variety of cavity loading methods, each with tradeoffs for fabrication simplicity and performance metrics. The second design, SBF-2, was an improvement of SBF-1, in which we increased the gain by

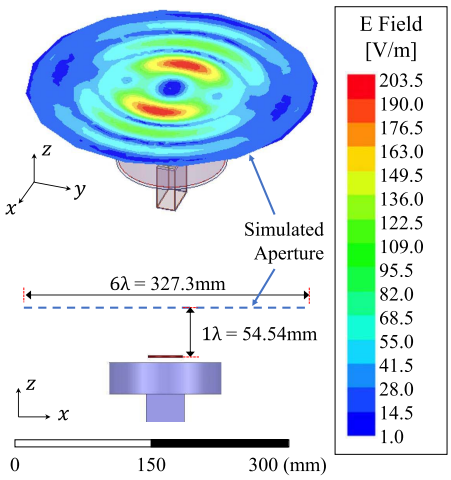

Fig. 3. SBF-1 aperture field distribution at 5.5 GHz.

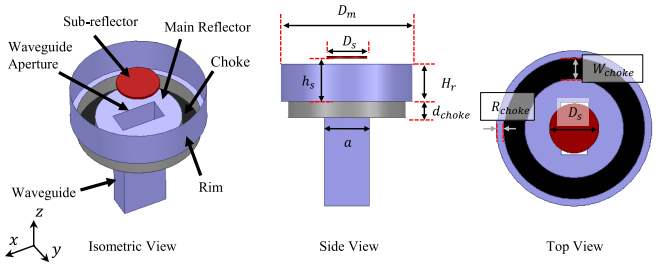

Fig. 4. SBF-2 geometry. Choke bottom and sides are shown in black and gray for clarity.

modifying the main reflector of the antenna with a choke. In a third design, SBF-2-Ring, we extended our results from SBF-2 by loading the cavity with a ring, which enhanced the impedance bandwidth, improved the aperture field distribution uniformity, and improved the cross-polarization performance. Our novel designs retain a compact structure while simultaneously improving gain, impedance bandwidth, and cross-polarization performance.

B. SBF-2 Design

Building on the past research on conventional SBF antennas, we sought methods to increase the gain of the antenna by modifying the main reflector geometry. Simulations of the SBF-1 antenna showed that the surface current distribution on the main reflector surface was primarily focused near the wide edges of the waveguide feed. We modified the surface to have a single corrugation, which is also known as a "choke." The idea of adding a choke to the main reflector beside the rim was first introduced in [17]; however, to the authors' knowledge, there have been no further reported studies on it. The geometry of the design is shown in Fig. 4. A choke, with width W_{choke}, depth d_{choke}, and distance from the outer rim, R_{choke}, has been introduced into the bottom of the main reflector.

We performed parametric studies on the choke dimension to find configurations that met the gain requirement at our desired frequency of operation 5.5 GHz. From these results,

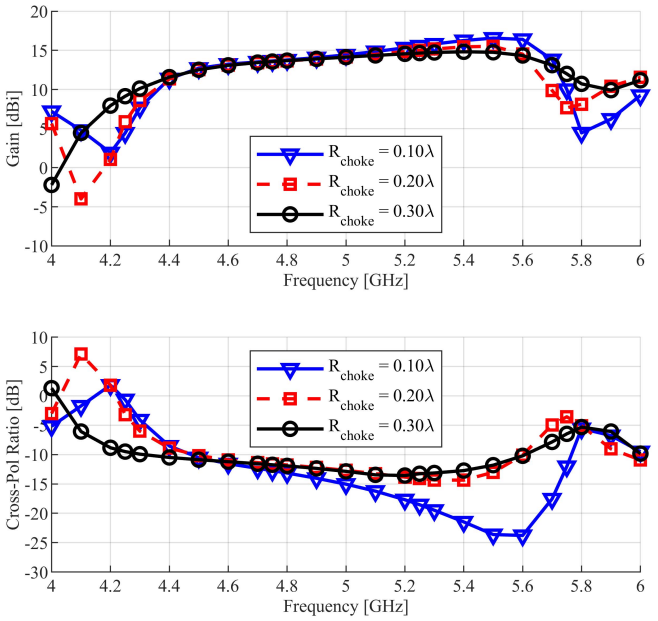

Fig. 5. SBF-2—gain variation for $\varphi = 0°$ (top) and worst case cross-polarization ratio ($\varphi = 46°$) (bottom) as a function of spacing between choke and outer rim edge (R_{choke}). $W_{choke} = 0.3\lambda$ and $d_{choke} = 0.3\lambda$.

we analyzed the S_{11} simulations and selected design configurations that met both the bandwidth and frequency metrics (see Table I). We also considered the worst case cross-polarization ratio in our analyses. Later, in Section III, we show the construction of one of the designs that has the highest gain and widest impedance bandwidth for the SBF-2 configuration.

In our parametric studies, we varied the gap between the rim and the outer diameter of the choke (R_{choke}), the depth of the choke (d_{choke}), and the choke width (W_{choke}). All other parameters were kept constant. Several candidate configurations met the requirements and we determined that we needed to constrain the values, as follows: $R_{choke} \leq 0.2\lambda$, $0.2\lambda \leq d_{choke} \leq 0.3\lambda$, and $0.2\lambda \leq W_{choke} \leq 0.3\lambda$.

As a demonstration of one of the parametric studies, Fig. 5 shows the realized gain and worst case cross-polarization ratio, while Fig. 6 shows the S_{11} plot for fixed values of W_{choke} and d_{choke}, while R_{choke} is varied. The results in Fig. 5 demonstrate that $R_{choke} = 0.1\lambda$ gives the highest gain, with a value of 16.6 dBi at 5.5 GHz. The configuration with $R_{choke} = 0.1\lambda$ affords the widest impedance bandwidth of operation (800 MHz, from 4.9 to 5.7 GHz, or 15.1%) that meets the gain specification. Using the 3 dB gain definition, the bandwidth of operation extends from 4.7 to 5.7 GHz or 19.2%. Simultaneously, the cross-polarization ratio is less than -14 dB for the same frequency range, with a minimum value of -23.8 dB at 5.6 GHz.

The S_{11} plots in Fig. 6 exhibit two resonances. One is at 5.5 GHz, the primary design frequency, and a second resonance can be seen at a lower frequency. Reducing R_{choke} corresponds to increasing the choke diameter. This results in a downward frequency shift and a resultant increase in impedance bandwidth. Further reduction of R_{choke} pushed the curve above -10 dB for 5–5.2 GHz, which was not an

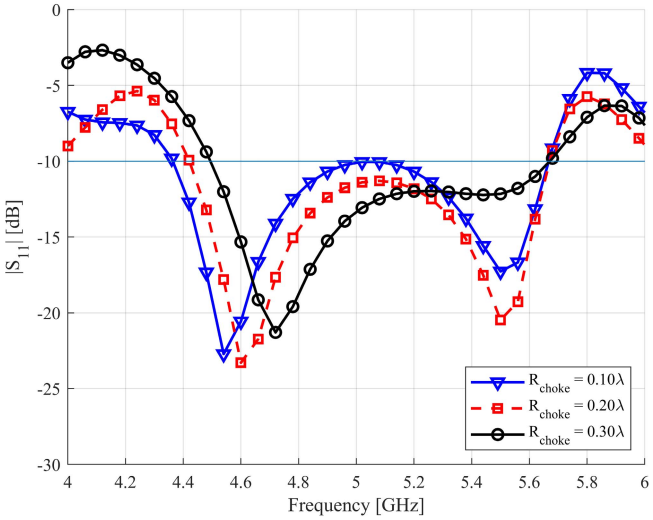

Fig. 6. SBF-2—S_{11} variation as a function of spacing between choke and outer rim edge (R_{choke}). $W_{choke} = 0.3\lambda$ and $d_{choke} = 0.3\lambda$.

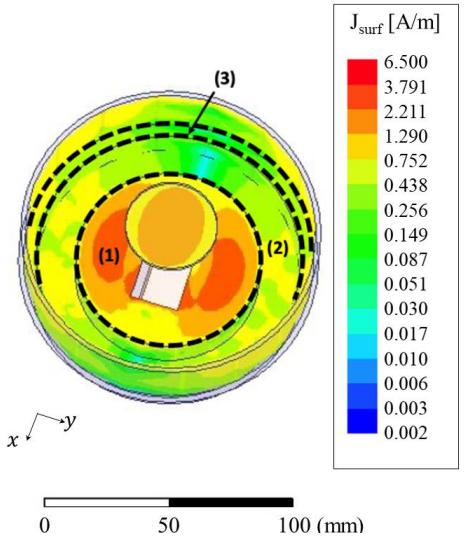

Fig. 7. SBF-2 surface current distribution for 5.5 GHz. Regions (1) and (3)—main reflector. Region (2)—choke.

acceptable design. The impedance bandwidth of operation for the configuration with $R_{choke} = 0.1\lambda$ was 1.3 GHz (from 4.4 to 5.7 GHz or 25.7%); however, as stated for the gain specification, the actual operation is constrained by the gain performance. It should be noted that in our design study, we used the antenna parameters to broaden its impedance bandwidth, rather than using a separate impedance matching section that could reduce antenna gain and efficiency.

Fig. 7 shows the surface current distribution for SBF-2. By virtue of the current distribution, each of the antenna components (i.e., the main reflector, subreflector, and rim) contributes to the radiation. The main reflector surface current was primarily concentrated in the region that was in closest proximity to the waveguide [region (1)]. The choke contribution [region (2)] to the radiation is the smallest among the three areas of the main reflector. The surface current magnitude of the section of main reflector that is beside the rim [region (3)] is approximately 1/6 of region (1). The surface current was partially constrained to region (2), due to the presence of the choke. As a result, the concentration of the current yields a more focused pattern and, consequently, a higher realized gain than designs without the choke.

The aperture field distribution at 5.5 GHz for SBF-2 is given in Fig. 8. In comparison to SBF-1 (Fig. 3), we note that while the peak field magnitudes are immediately above the waveguide aperture, the field magnitudes are more equally distributed across the main reflector aperture. This results in a higher gain and lower cross polarization than SBF-1.

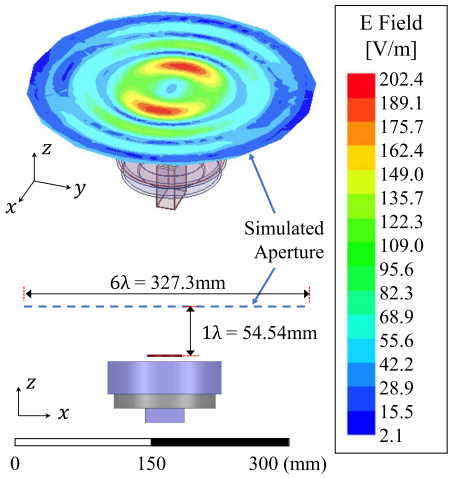

Fig. 8. SBF-2 aperture field distribution at 5.5 GHz.

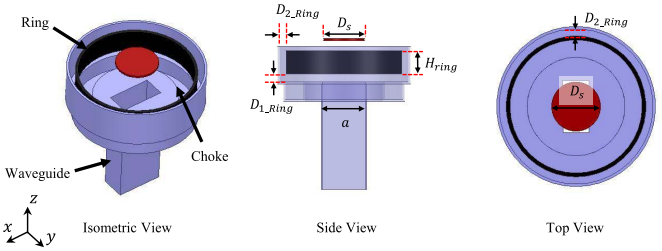

Fig. 9. SBF-2-Ring geometry. Ring material is shown in black for clarity.

C. SBF-2-Ring Design

In this section, we present a method for enhancing the cross-polarization performance and antenna impedance bandwidth through a modification of the SBF-2 structure. There are some applications in which antenna impedance bandwidth is more important than the gain, and a small sacrifice in gain performance can be traded for a much broader impedance bandwidth. The technique was a simple, elegant, and effective modification of the SBF-2 design. It involved adding a conductive ring within the rim. The ring diameter was slightly smaller than the main outer diameter, and as a result, a mode of operation at a higher frequency was added. In addition, the presence of the ring changed the current distribution of SBF-2 on the rim, resulting in a better cross-polarization result (as will be seen in the experimental verification). SBF-2-Ring geometries are shown in Fig. 9.

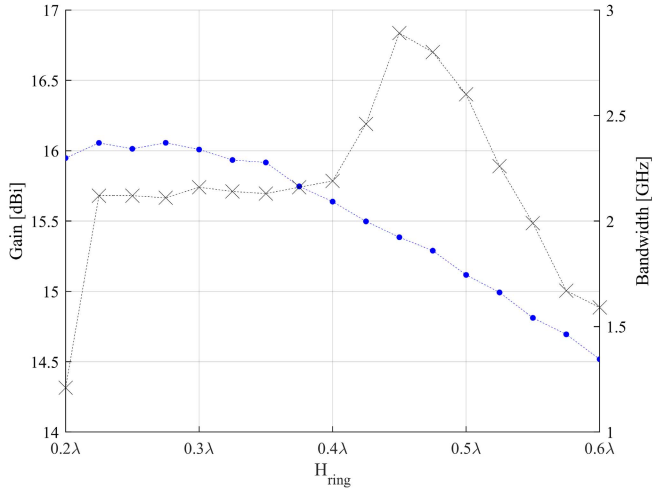

Fig. 10. SBF-2-Ring—gain for $\varphi = 0°$ at 5.5 GHz (symbol: •) and impedance bandwidth (symbol: x) variation as a function of ring height (H_{ring}). $D_{1-ring} = 0$ and $D_{2-ring} = 0.05\lambda$.

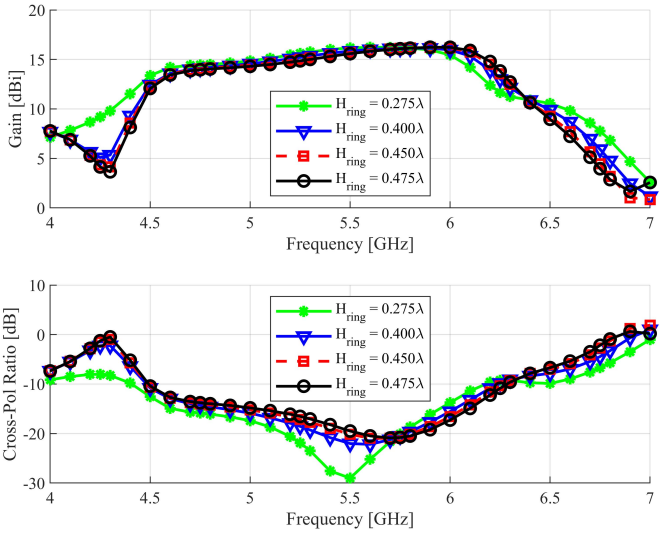

Fig. 11. SBF-2-Ring—gain variation for $\varphi = 0°$ (top) and worst case cross-polarization ratio $\varphi = 46°$ (bottom) as a function of ring height (H_{ring}). $D_{1-ring} = 0$ and $D_{2-ring} = 0.05\lambda$.

In our parametric studies, we varied the ring height (H_{ring}), the distance between the ring and the main reflector (D_{1-ring}), and the distance between the ring and the rim (D_{2-ring}). The ring thickness was set to a constant (2 mm) in the simulations. During the parametric study, all other dimensions of SBF-2-Ring were held constant.

The variation in gain as a function of ring height at the design frequency of 5.5 GHz is shown in Fig. 10. An increase in ring height results in a gradual decrease of gain. At the same time, the impedance bandwidth shows a marked increase between 0.400λ and 0.525λ. The peak impedance bandwidth was at 0.450λ; however, the S_{11} curve was equal to -10 dB for several frequencies, meaning that there was no margin for error in the fabrication process. The maximum gain was found with ring height (H_{ring}) at 0.275λ. Therefore, a design tradeoff between impedance bandwidth and gain performance must be made and will be application-specific.

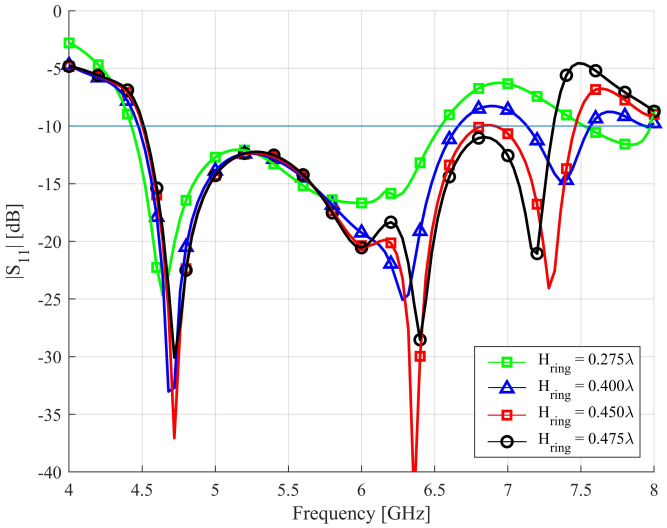

Fig. 12. SBF-2-Ring—S_{11} variation as a function of ring height (H_{ring}). $D_{1-ring} = 0$ and $D_{2-ring} = 0.05\lambda$.

Fig. 11 Shows the Gain Variation as a Function of the Ring Height for $D_{1-ring} = 0$ and $D_{2-ring} = 0.05\lambda$. We Present These Particular Ring Heights Based on the Results in Fig. 10, Where $H_{ring} = 0.275\lambda$ Had the Highest Gain and the Impedance Bandwidth for Ring Heights Between 0.400λ and 0.525λ Was Significantly Larger Than Other Heights. The Gain Results in Fig. 11 Illustrate That the Gain Bandwidth of Operation Was 1.5 GHz (e.g., From 4.7 to 6.2 GHz, or 27.5%, for $H_{ring} = 0.4\lambda$) and the Ring Height Did Not Significantly Affect the Realized Gain Magnitude (it Was 16.2 dBi Maximum for Each of the cases). Using the 3 dB gain definition, the bandwidth of operation extends from 4.5 to 6.2 GHz or 31.8%. Simultaneously, the cross-polarization ratio was <-11 dB for the same frequency range, with a minimum value of -29.0 dB at 5.5 GHz. For comparison with SBF-2, we examined the same bandwidth (4.9–5.7 GHz) and the cross-polarization ratio was <-15.2 dB. On average, the ratio was -18.7 dB for SBF-2 and -19.0 dB for SBF-2-Ring. Therefore, the SBF-2-Ring configuration had a better cross-polarization performance in all respects. Since the initial design goal of SBF-2-Ring was to increase the impedance bandwidth, the approach was successful.

Fig. 12 shows the S_{11} plots, in which we varied the ring height (H_{ring}) and kept $D_{1-ring} = 0$ and $D_{2-ring} = 0.05\lambda$. Note that in this figure, the frequency axis extends to 8 GHz, whereas the axis for SBF-2 only went up to 6 GHz. Similar to SBF-2, the antenna exhibits a resonance at around 4.7 GHz; however, the addition of the ring has made a significant change at frequencies greater than 5.5 GHz. A dual resonance behavior appears, with a notch between 6 and 6.5 GHz and another at 7.3 GHz. This behavior is more pronounced for ring heights $\geq 0.400\lambda$, but it is still evident for the $H_{ring} = 0.275\lambda$ (maximum gain) case. For substantially shorter and taller rings, the impedance bandwidth was similar to SBF-2, and thus, these results are not shown.

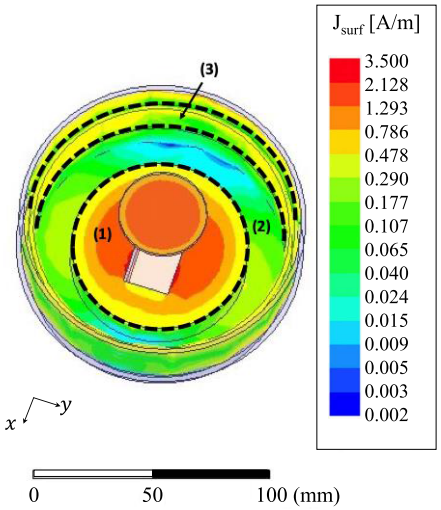

Fig. 13. SBF-2-Ring surface current distribution for 5.5 GHz. Regions (1) and (3)—main reflector. Region (2)—choke.

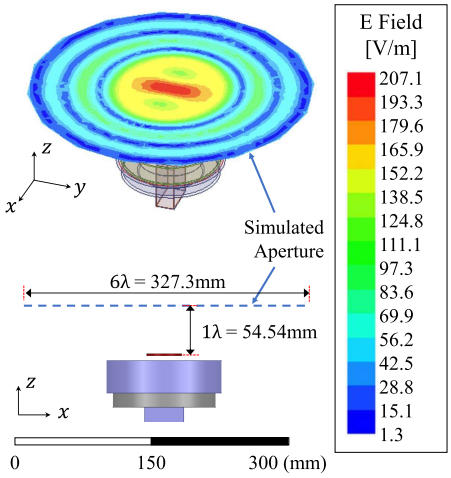

Fig. 14. SBF-2-Ring aperture field distribution at 5.5 GHz.

We determined that the maximum impedance bandwidth (4.5–7 GHz or 43.5%) and gain bandwidth (1.5 GHz or 27.5%) required us to constrain the values as follows: $0.4\lambda \leq H_{ring} \leq 0.475\lambda$, $D_{1-ring} \leq 0.1\lambda$, and $0.05\lambda \leq D_{2-ring} \leq 0.1\lambda$. In other words, the ring needed to be shorter than the outer rim and could not be in contact with it. Contacting the bottom of the main reflector had no detrimental effect.

The surface current distribution of SBF-2-Ring is shown in Fig. 13. In comparison with SBF-2, adding the ring beside the rim altered the current distribution on the rim. In this design, similar to SBF-2, the majority of radiation came from the main reflector. The addition of the ring resulted in a uniform distribution of the current in the area between the ring and the top of the rim, and a new, higher frequency mode of operation, was introduced. This extended the impedance bandwidth of operation significantly.

The aperture field distribution at 5.5 GHz for SBF-2-Ring is given in Fig. 14. In comparison to SBF-2 (Fig. 8), the field magnitudes do not have the drastically higher field magnitudes

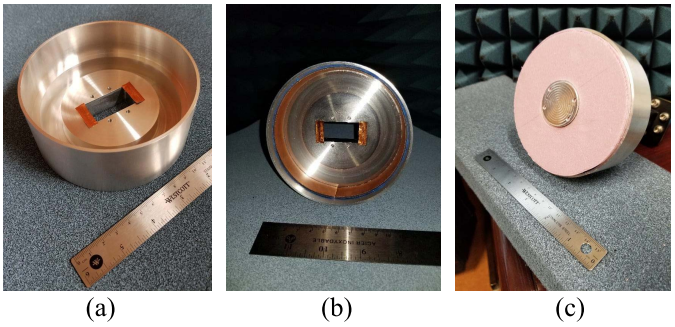

Fig. 15. Fabricated SBF antenna. (a) SBF-2: view of main reflector with iris for impedance matching. (b) SBF-2-Ring: main reflector with ring visible. (c) SBF-2: fully assembled design.

TABLE II
FABRICATED ANTENNA DIMENSIONS

Parameter	Description	Relative	Absolute
D_m	Main reflector diameter	2.2λ	120 mm
D_s	Sub-reflector diameter	0.7λ	38.181 mm
H_r	Rim height	0.6λ	32.727 mm
hs	Height of sub-reflector	0.7λ	38.181 mm
R_{choke}	Gap between rim and outer diameter of choke	0.1λ	5.455 mm
d_{choke}	Depth of the choke	0.3λ	16.364 mm
W_{choke}	Width of choke	0.3λ	16.364 mm
H_{ring}	Ring height	0.4λ	21.818 mm
$D_{1\text{-ring}}$	Ring distance from main reflector	0λ	0 mm
$D_{2\text{-ring}}$	Ring distance from rim	0.05λ	2.727 mm

immediately above and beside the waveguide aperture. In fact, the field appears to exhibit a radial symmetry. The symmetry results in a significant improvement in cross polarization when compared with SBF-2.

III. Antenna Prototype Fabrication and Test

In order to verify the antenna simulations, we built prototypes of the designs. Throughout our design process, we considered practical fabrication aspects. Components were constructed in our machine shop using traditional metalworking methods. We chose aluminum for its low mass and ease in fabrication processes. Our machinist did not optimize the mass of the antenna at this stage, as the primary goal was performance verification. Consequently, the SBF-2 and SBF-2-Ring designs could be significantly reduced by trimming additional material in a future build. The mass of SBF-2 and SBF-2-Ring was 462.5 and 482.0 g, respectively. To position the subreflector at the desired height, we used a piece of foam material ($\varepsilon_r \approx 1.05$) that was cut to fit the interior of the cavity. We adapted our simulation geometry to include the segment of foam for appropriate comparison. All simulation results presented in this section incorporate the foam material. The main reflector of the SBF-2 prototype is shown in Fig. 15(a), the SBF-2-Ring prototype is shown in Fig. 15(b), and the fully assembled antenna (SBF-2) is shown in Fig. 15(c). Dimensions for the fabricated prototypes are given in Table II.

Through further simulation studies, we established that the diameter of the main reflector (D_m), the height of the sub-reflector (h_s), and the subreflector tilt angle are the critical design parameters. For the diameter of the main reflector and

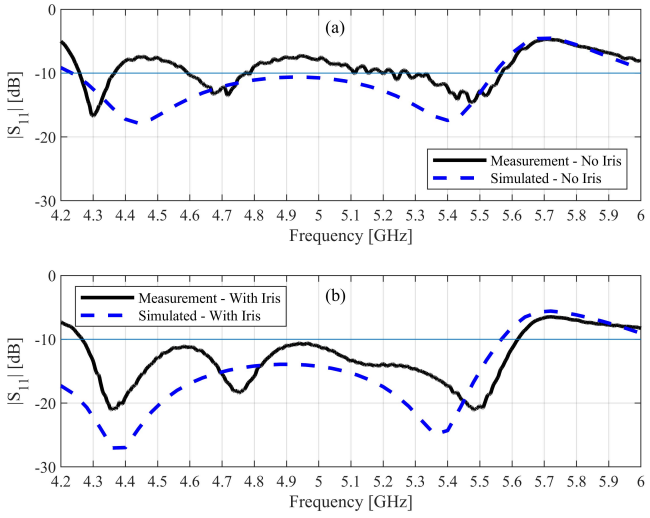

Fig. 16. SBF-2: S_{11} simulation and measurements.

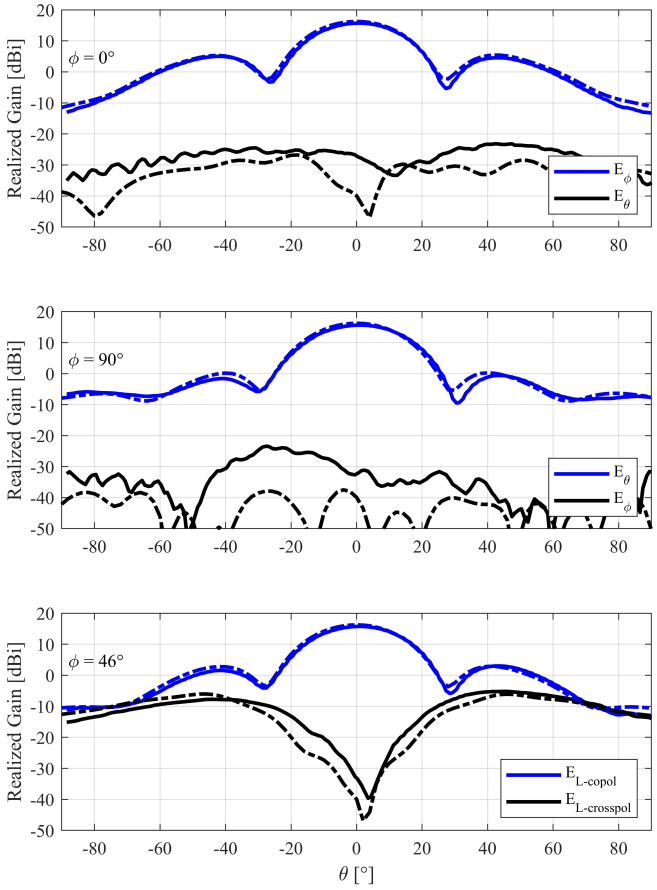

Fig. 17. SBF-2 radiation patterns at 5.5 GHz. Dashed lines show the simulated results and solid lines show measurements. In $\varphi = 46°$, the co- and cross-polarization patterns are according to Ludwig's 3rd definition [18].

the height of the subreflector, we recommend the tolerance of 1 and 0.5 mm for the fabrication, respectively. This should be relatively easy to achieve for a typical machine shop. Ideally, the subreflector should be perfectly parallel to the main reflector (i.e., a tilt angle of 0°). In actual fabrication, this can be challenging to attain. The error margin for the subreflector tilt angle should be limited to 5°.

We used an Agilent VNA (Model N5224B) to measure S_{11} for the prototype antennas. To connect the antennas to VNA, we used a low-cost commercial waveguide-to-coaxial adaptor, which fed its waveguide with a probe. It was therefore necessary to evaluate the performance of the adaptor first. This was done using two identical adaptors, connected back-to-back using a waveguide, and terminated in a matched load. The setup and the measurement results are shown in the Appendix. The results show that the adaptor S_{11} is satisfactory, as a quality test hardware, only for frequencies above 5.2 GHz. Below that, it represents a complex impedance, with multiple oscillations, which interact with the antenna input impedance, affecting its measured S_{11}, as shown in Fig 16(a). To improve S_{11} of the adaptor–antenna combination, so that the antenna gain and radiation patterns can be measured accurately, we added two strips of copper tape with conductive adhesive to the waveguide aperture, to create an inductive iris and lower the simulated antenna S_{11} to below -14 dB. The resulting S_{11} of the combined adaptor and antenna with the matching iris is compared with simulation in Fig. 16(b). It clearly shows the effects of the waveguide adaptor, but the combined results now remain below -10 dB, necessary for conducting the measurements. The details of the results are shown in the Appendix.

Experimentally, we found that the width of $\sim$4.5 mm was effective at improving the match. We added the strips in HFSS simulations to find the effect of the width and determined that values between 4 and 5 mm were all effective. The impedance bandwidth is 1.35 GHz (4.27–5.62 GHz or 27.3%); however, the operational bandwidth of the antenna is determined by the gain performance as well, so radiation pattern results were evaluated. We examined the effect of the iris on the far-field patterns and gain for both SBF-2 and SBF-2-Ring. The results showed a negligible difference.

The radiation patterns were measured in the University of Manitoba's Compact Antenna Test Range (CATR). Radiation patterns for SBF-2 at 5.5 GHz are shown in Fig. 17. The measured peak gain was 15.7 dBi and the simulated gain was 16.3 dBi. If we account for the 0.2 dB insertion loss from the waveguide to coaxial cable connector, the simulated and measured co-polarized radiation patterns are in excellent agreement (within 0.4 dB). The remaining difference can be attributed to the imperfect bonding between the waveguide flange and the bottom of the main reflector. Cross polarization was calculated using Ludwig's 3rd definition [18]. The peak value was at $\varphi = 46°$ and $\theta = 38°$, giving a worst case of -20.9 dB cross-polarization ratio.

We constructed the ring for SBF-2-Ring using a piece of flexible dielectric substrate ($\varepsilon_r \approx 2.5$) with copper cladding. A section of substrate material was trimmed, shaped into a ring, and installed in the SBF-2 main reflector. The ring height was 0.4λ (21.8 mm), the gap, D_{2-ring}, was 2 mm and the copper ring thickness was 0.035 mm (formed by the copper cladding on the substrate). This ring dimension was chosen as a compromise between gain performance and impedance bandwidth.

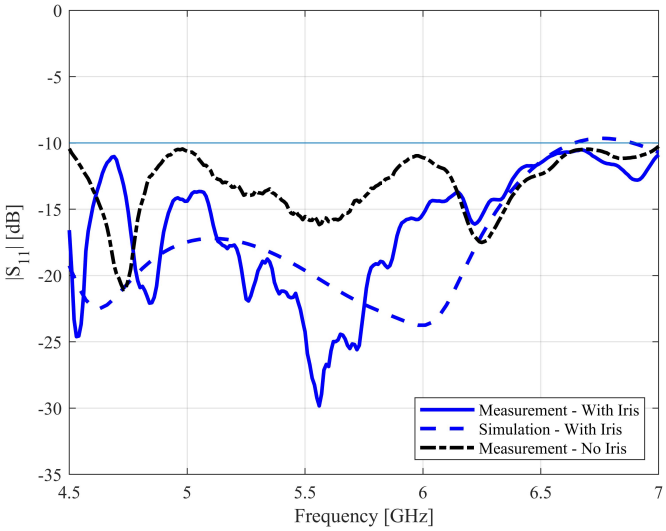

Fig. 18. SBF-2-Ring: S_{11} simulation and measurements.

Measured S_{11} results for SBF-2-Ring are shown in Fig. 18. Measurements with the inductive iris showed good performance, so we left it in place. Later, after radiation tests, we removed the iris to see the effect and the results shown in Fig. 18 indicate that the S_{11} profile degrades since the values increase substantially. We investigated the width of the strips in further HFSS simulations to find the effect of the width and determined that values between 4 and 5 mm were all effective at improving the impedance match. Notches in the S_{11} results occur at 4.84 and 5.56 GHz. The impedance bandwidth is 2.5 GHz (4.5–7.0 GHz or 43.5%). We note that for frequencies below 4.7 GHz, the S_{11} measurement is influenced by performance of the waveguide-to-coaxial adaptor.

Radiation patterns for SBF-2-Ring at 5.5 GHz are shown in Fig. 19. The measured peak gain was 15.6 dBi and the simulated gain was 15.8 dBi. Again, the simulated and measured co-polarized radiation patterns are in excellent agreement (peak values are within 0.1 dB, if we account for the waveguide adaptor loss of 0.2 dB). Cross polarization was calculated using Ludwig's 3rd definition and the peak value was at $\varphi = 46°$ and $\theta = -45°$, giving a worst case of -29.1 dB cross-polarization ratio.

Radiation patterns were measured in a range of frequencies and we present the results from 4.9 to 5.8 GHz in Fig. 20. SBF-2 gain and worst case cross-polarization measurement results were in good agreement with simulation, including a drop-off for frequencies above 5.6 GHz (see Fig. 5, $R_{choke} = 0.1\lambda$). SBF-2-Ring gain performance was similar in magnitude to SBF-2, but there was a near-constant gain value across the entire measurement bandwidth. Worst case cross polarization was similar to simulation for frequencies below 5.2 GHz. The cross-polarization measurements were excellent (<-22 dB) between 5.3 and 5.8 GHz. The SBF-2-Ring design has met all of the proposed specifications.

For comparison with other published designs, we have provided a summary in Table III. Column 1 gives a description of the antenna construction/excitation. The impedance bandwidth is given as a percentage, following the standard definition.

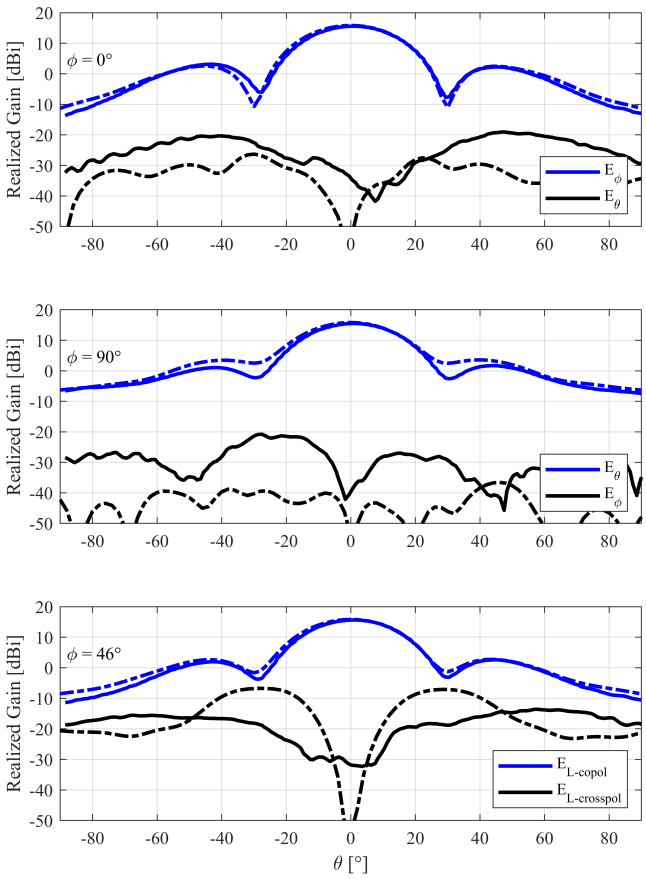

Fig. 19. SBF-2-Ring radiation patterns at 5.5 GHz. Dashed lines show simulated results and solid lines show measurements. In $\varphi = 46°$, the co- and cross-polarization patterns are according to Ludwig's 3rd definition [18].

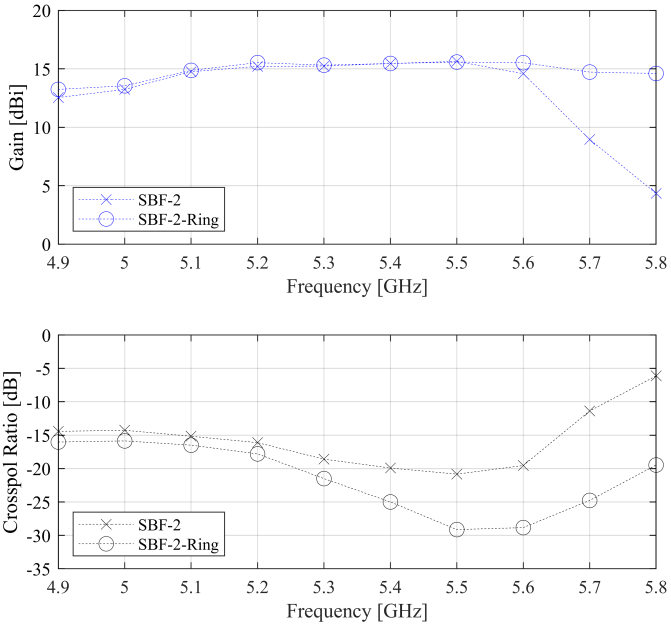

Fig. 20. Measured gain and worst case cross-polarization ratio for SBF-2 and SBF-2-Ring.

The maximum gain, Gmax in dBi, is given next. The antenna volume, which is expressed in electrical units, relative to the reported design frequency, is given. Finally, the reference for

TABLE III
COMPARISON OF BANDWIDTH, PEAK GAIN, AND VOLUME WITH OTHER SBF ANTENNA DESIGNS

Description	Impedance BW [%]	Peak Gain [dBi]	Volume	Ref.
SBF-1. Waveguide fed, flat reflector	26.4	14.9	$0.84\pi\lambda_0^3$	This Work
SBF-2. Choke on main reflector	27.3	16.6	$1.21\pi\lambda_0^3$	This Work
SBF-2-Ring. SBF-2 with metallic ring	43.5	15.8	$1.21\pi\lambda_0^3$	This Work
Cavity-backed folded triangular bowtie antenna	92.2	9.5	$0.14\pi\lambda_0^3$	[6]
Excited by unbalanced-fed H-shaped slot	20	15.5	$0.70\pi\lambda_0^3$	[8]
Waveguide fed broadband millimeter wave	57	18.5	$2.58\pi\lambda_0^3$	[12]
Backfire microstrip patch antenna feed	52.8	6.0	$0.15\pi\lambda_0^3$	[13]
Coaxial waveguide fed	10	18.0	$0.87\pi\lambda_0^3$	[16]
Waveguide fed, corrugated rim	10	20.8	$1.13\pi\lambda_0^3$	[19]
Waveguide fed, parasitic wires, flat reflector	10	16.2	$0.5\pi\lambda_0^3$	[20]

each design is reported in the last column. Note that in this table, we presented the impedance bandwidth using regularly reported metric of $|S_{11}| < -10$ dB. We are unable to provide a good comparison for cross polarization, as reported values and levels are somewhat inconsistent in the literature.

From this summary table, we note that small volume antennas can achieve high-impedance bandwidth, but at the cost of low peak gain (e.g., [6], [13]). Some of the designs with the highest gain had the lowest reported bandwidth (e.g., [16], [19], [20]). In comparison, our designs show a good compromise between achieved bandwidth and gain while still maintaining a moderate volume (e.g., [12] has higher gain and bandwidth, but it is more than twice the volume of our antenna).

IV. CONCLUSION

We presented innovative designs, which improves the gain and cross-polarization performance of the waveguide-fed SBF antenna. Our emphasis was on improving design aspects for compact, low profile, and low mass antennas that are simple to construct and can be used for operation in the microwave C-band. We have succeeded in meeting design specifications for such an antenna.

The first design, called SBF-1, had a flat main reflector. We presented these results as a benchmark for the improvements proposed and presented here. The second design, called the SBF-2 antenna, had a choke feature in the main reflector that concentrated the current distribution and resulted in an increase in realized gain when compared to the typical flat main reflector. The bandwidth of operation that met the gain specification of 14 dBi was 800 MHz (from 4.9 to 5.7 GHz or 15.1%), with a peak value of 16.6 dBi. Using the 3 dB gain definition, the bandwidth of operation extends from 4.7 to 5.7 GHz or 19.2%. Cross-polarization ratios were moderate throughout the design bandwidth (<-14 dB) and reached a simulated minimum of -23.8 dB at 5.6 GHz. Principal plane ratios were significantly better, as expected theoretically, and shown in the measurement results. We examined the input impedance and S_{11} results showed that the impedance bandwidth was significantly larger than the gain bandwidth and was therefore not a limiting factor on the performance. For SBF-2, the peak gain was 16.6 dBi, the minimum cross-polarization ratio was -23.8 dB, and the maximum impedance bandwidth was 27.3%.

The second innovation, called the SBF-2-Ring, added a ring feature to the SBF-2 design. The ring diameter was slightly smaller than the main rim and this extended operation to a higher frequency. The bandwidth of operation that met the gain specification of 14 dBi was 1.5 GHz (from 4.7 to 6.2 GHz or 27.5%). Using the 3 dB gain definition, the bandwidth of operation extends from 4.5 to 6.2 GHz or 31.8%. Cross-polarization ratios were moderate throughout the design bandwidth and were better than SBF-2 across the same band (<-15.2 dB). They reached a simulated minimum of -29.0 dB and measured minimum of -29.1 dB at 5.5 GHz. In general, the SBF-2-Ring configuration has a better cross-polarization performance than SBF-2. We examined the input impedance and S_{11} results showed that the impedance bandwidth was significantly larger than the gain bandwidth (approximately 300% larger), and the addition of the ring resulted in a uniform distribution of current in the region between the ring and the waveguide. For SBF-2-Ring, the peak gain was 15.8 dBi, the minimum cross-polarization ratio was -29.1 dB, and the maximum impedance bandwidth was 43.5%.

Prototypes of each design were fabricated and tested. Excellent agreement between simulation and measurement results was achieved for both SBF-2 and SBF-2-Ring. The optimized SBF-2-Ring met all of the performance specifications. It operated with moderate gain (>14 dBi) and had a good cross-polarization ratio (<-22 dB), and over 500 MHz bandwidth. With appropriate selection of the SBF geometry and cavity loading, as described in this article, many usable configurations can be obtained.

From these results, we plan to use the antenna in remote sensing systems. Future work will include adding dual-polarization capability, reducing mass, and enhancing gain.

APPENDIX
ANALYSIS OF WAVEGUIDE ADAPTORS

In our design, we proposed to use WR159 as the main waveguide feed. Our design specifications have a primary operating frequency at 5.5 GHz and a bandwidth of 500 MHz. We chose this standard waveguide size because its recommended operating frequency is 4.90–7.05 GHz and would ideally meet these specifications. In our design, we were able to show by simulation that the antenna would operate at lower frequencies (i.e., down to 4.4 GHz). In HFSS, the simulation assumes an ideal TE10 mode operation for the waveguide when it is fed with a port excitation.

We performed additional measurements on the waveguide and adaptors, as shown in Fig. 21. The results of the measurements are given in Fig. 22, in comparison with the antenna simulations.

Fig. 21. Waveguide and adaptors under test in the Antennas Lab.

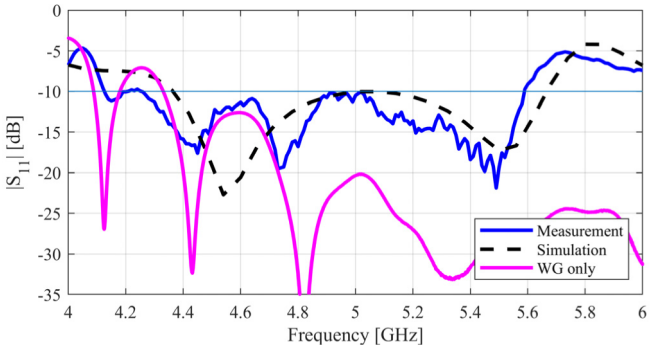

Fig. 22. Comparison of SBF-2 measurement, SBF-2 simulation, and WG plus adaptors.

Referring to Fig. 16, when we looked at the S_{11} results for the SBF-2 antenna measurement, we noticed that there were notches at 4.125, 4.43, and 4.82 GHz. At ~4.6 GHz, there was a local maximum in the measurement, which was not present in the simulation results. To find the discrepancy, we measured S_{11} for the waveguide and adaptors (setup as shown in Fig. 21) and the results are shown as the "WG only" curve in Fig. 22. The notches at 4.125, 4.43, and 4.82 GHz are visible in the WG measurement. Furthermore, we can see that at 4.6 GHz, the waveguide has a local maximum in S_{11} at 4.6 GHz. The antenna measurement follows this. Thus, it appears that the WG (and namely the WG adaptor) is the cause of this discrepancy. It is clear that the antenna measurement is influenced by the waveguide adaptor for frequencies less than 4.7 GHz.

ACKNOWLEDGMENT

The authors would like to thank Ehsan Zeynali and Cory Smit for their assistance in antenna fabrication and test. They would also like to thank CMC Microsystems for the provision of CAD tools that facilitated this research.

REFERENCES

[1] H. Ehrenspeck, "The backfire antenna, a new type of directional line source," *Proc. IRE*, vol. 48, no. 1, pp. 109–110, 1960.
[2] H. W. Ehrenspeck, "The short-backfire antenna," *Proc. IEEE*, vol. 53, no. 8, pp. 1138–1140, Aug. 1965, doi: 10.1109/PROC.1965.4119.
[3] S. Yang, S. H. Tan, and J. S. Fu, "Short backfire antennas for wireless LAN applications at millimeter-waves," in *Proc. IEEE Intl. Symp. Antennas Propag.*, Jul. 2000, pp. 1260–1262.
[4] E. Nielsen and K. Pontoppidan, "Backfire antennas with dipole elements," *IEEE Trans. Antennas Propag.*, vol. AP-18, no. 3, pp. 367–374, May 1970.
[5] R. Li, D. C. Thompson, J. Papapolymerou, J. Laskar, andM. M. Tentzeris, "A circularly polarized short backfire antenna excited by an unbalance-fed cross aperture," *IEEE Trans. Antennas Propag.*, vol. 54, no. 3, pp. 852–859, Mar. 2006.
[6] S. W. Qu, J. L. Li, Q. Xue, C. H. Chan, and S. M. Li, "Wideband and unidirectional cavity-backed folded triangular bowtie antenna," *IEEE Trans. Antennas Propag.*, vol. 57, no. 4, pp. 1259–1263, Apr. 2009.
[7] D. Gray and H. Tsuji, "Short backfire antenna with microstrip Clavin feed," *IET Microw., Antennas Propag.*, vol. 3, no. 8, pp. 1211–1217, Dec. 2009.
[8] R. Li, D. Thompson, M. M. Tentzeris, J. Laskar, and J. Papapolymerou, "Development of a wide-band short backfire antenna excited by an unbalance-fed H-shaped slot," *IEEE Trans. Antennas Propag.*, vol. 53, no. 2, pp. 662–671, Feb. 2005.
[9] S. W. Qu, J. L. Li, Q. Xue, and C. H. Chan, "Wideband cavity-backed bowtie antenna with pattern improvement," *IEEE Trans. Antennas Propag.*, vol. 56, no. 12, pp. 3850–3854, Dec. 2008.
[10] J. A. Nessel, C. L. Kory, K. M. Lambert, R. J. Acosta, and F. A. Miranda, "A microstrip patch-fed short backfire antenna for the tracking and data relay satellite system-continuation (TDRSS-C) multiple access (MA) array," in *Proc. IEEE Antennas Propag. Soc. Int. Symp.*, Albuquerque, NM, USA, Jul. 2006, pp. 521–524.
[11] Y. Yamada, T. Takan, and N. Ishida, "Compact antenna equipment for maritime satellite communication systems," *Trans. IEICE*, vol. 62, pp. 844–846, Jun. 1979.
[12] S.-W. Qu, K. B. Ng, and C. H. Chan, "Waveguide fed broadband millimeter wave short backfire antenna," *IEEE Trans. Antennas Propag.*, vol. 61, no. 4, pp. 1697–1703, Apr. 2013.
[13] P. Gour and R. Mishra, "Bandwidth enhancement of a backfire microstrip patch antenna for pervasive communication," *Int. J. Antennas Propag.*, vol. 2014, Jan. 2014, Art. no. 560185.
[14] G. S. Kirov, "Design of short backfire antennas," *IEEE Antennas Propag. Mag.*, vol. 51, no. 6, pp. 110–120, Dec. 2009.
[15] A. Mansoori and D. Isleifson, "Design of short backfire antennas for remote sensing applications," in *Proc. IEEE 19th Int. Symp. Antenna Technol. Appl. Electromagn. (ANTEM)*, Winnipeg, MB, Canada, Aug. 2021, pp. 1–2.
[16] A. A. Kishk and L. Shafai, "Performance of short-backfire antenna with different excitation sources," *Int. J. Electron.*, vol. 63, no. 6, pp. 825–832, Dec. 1987.
[17] D. P. Gray and L. Shafai, "Parametric study of short backfire antennas with different cavity profiles," in *Proc. IEEE Antennas Propag. Soc. Int. Symp.*, Aug. 2000, pp. 1314–1317.
[18] A. Ludwig, "The definition of cross polarization," *IEEE Trans. Antennas Propag.*, vol. AP-21, no. 1, pp. 116–119, Jan. 1973.
[19] M. S. Leong and P. S. Kooi, "Rectangular-waveguide-excited short backfire antenna with corrugated rim," *Electron. Lett.*, vol. 15, no. 17, pp. 533–535, Aug. 1979, doi: 10.1049/el:19790384.
[20] D. Gray, H. Tsuji, and Y. Fujino, "Waveguide fed short backfire antennas with parasitic wires," in *Proc. Int. Symp. Antennas Propag.*, Jun. 2009, pp. 1–4, doi: 10.1109/APS.2009.5171673.

Amirbahador Mansoori (Student Member, IEEE) received the B.Sc. degree in electrical and computer engineering with a minor in telecommunications engineering from Shahid Beheshti University, Tehran, Iran, in 2017, and the M.Sc. degree from the Department of Electrical and Computer Engineering, University of Manitoba, Winnipeg, MB, Canada, in 2021.

He has been involved in the academic community, including being part of the organizing team of the ANTEM 2021 conference and several IEEE talks, being a semi-finalist in 3MT competition, and publishing several papers. Since 2021, he has been working as an RF Research and Development Engineer at Acentury, Inc., Richmond Hill, ON, Canada, where he works on antenna and filter designs and SynMatrix automation filter design software. His research interests are RF component design including antenna and filter designs, applications of artificial intelligence in engineering designs, applied electromagnetics, and remote sensing.

Dustin Isleifson (Senior Member, IEEE) received the B.Sc. degree (Hons.) in electrical engineering and the Ph.D. degree in electrical and computer engineering from the University of Manitoba, Winnipeg, MB, Canada, in 2005 and 2011, respectively.

From 2013 to 2016, he was an Electrical Engineer with the Space Systems Department, Magellan Aerospace, Winnipeg, where he worked on the Radarsat Constellation Mission (RCM). Since 2016, he has been an Assistant Professor with the Department of Electrical and Computer Engineering, in a joint appointment with the Centre for Earth Observation Science (CEOS), University of Manitoba. His research interests include remote sensing, Arctic science, antenna design, and satellite technologies for remote sensing.

Dr. Isleifson was the Conference Co-Chair of IEEE ANTEM 2021 and the 19th International Symposium on Antenna Technology and Applied Electromagnetics. He is currently the Chapter Chair of the Winnipeg Section of the IEEE GRS/AES.

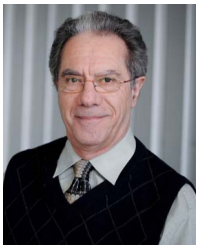

Lotfollah Shafai (Life Fellow, IEEE) received the B.Sc. degree from the University of Tehran, Tehran, Iran, in 1963, and the M.Sc. and Ph.D. degrees from the University of Toronto, Toronto, ON, Canada, in 1966 and 1969, respectively.

In November 1969, he joined the Department of Electrical and Computer Engineering, University of Manitoba, Winnipeg, MB, Canada, as a Lecturer, where he was an Assistant Professor in 1970, an Associate Professor in 1973, a Professor in 1979, a Distinguished Professor in 2002, and a Distinguished Professor Emeritus in 2016. His assistance to industry was instrumental in establishing an Industrial Research Chair in Applied Electromagnetics at the University of Manitoba in 1989, which he held until July 1994.

Dr. Shafai is a Life Fellow of The Royal Society of Canada. In 2002, he was elected as a fellow of The Canadian Academy of Engineering and a Distinguished Professor at the University of Manitoba. In 2009, he was elected as a fellow of the Engineering Institute of Canada. He was a recipient of numerous awards. In 1978, his contribution to the design of the first miniaturized satellite terminal for the Hermes satellite was selected as the Meritorious Industrial Design. He received the Professional Engineers Merit Award in 1984, "The Thinker" Award from Canadian Patents and Development Corporation in 1985, the Maxwell Premium Award from IEE, London, in 1990, the Distinguished Achievement Awards from Corporate Higher Education Forum in 1993 and 1994, the Winnipeg RH Institute Foundation Medal for Excellence in Research in 1998, and the University of Manitoba Research Award in 1999 and 2000. From the University of Manitoba, he received the "Research Awards" in 1983, 1987, and 1989, the Outreach Award in 1987, and the Sigma Xi Senior Scientist Award in 1989. He was a recipient of the IEEE Third Millenium Medal in 2000, the IEEE Chen-To-Tai Distinguished Educator Award, the Edward E. Altschuler Best Paper Prize from *IEEE APS Magazine* in 2014, the Best Paper Award from IEEE ANTEM in 2016, and the IEEE Antennas and Propagation Society's Distinguished Achievement Award "for contributions to singular electromagnetics, moment methods, reflector feeds and virtual arrays, wideband antennas, gain enhancement in miniaturized antennas, and dielectric film circuits and antennas" in 2018. He received the IEEE Canada "Reginald A. Fessenden Medal" for "outstanding contributions to telecommunications and satellite communications" and the Natural Sciences and Engineering Research Council (NSERC) Synergy Award for "development of advanced satellite and wireless antennas" in 2003, the Killam Prize in Engineering from The Canada Council for his "outstanding Canadian career achievements in engineering and his research on antennas" in 2011, and The "John Kraus antenna Award" from IEEE Antennas and Propagation Society "for contributions to the design and understanding of small high-efficiency feeds and terminals, wideband planar antennas, low-loss conductors, and virtual array antennas" in 2013. He held a Canada Research Chair in applied electromagnetics from 2001 to 2016 and was the International Chair of Commission B of the International Union of Radio Science (URSI) from 2005 to 2008. In 2017, the International Union of Radio Science, URSI, awarded him the Booker Gold Medal "for outstanding contributions to antenna miniaturization by electromagnetics and numerical techniques, small satellite terminals, planar antennas, invention of virtual reflectors, low-loss engineered conductors, and dielectric film components and antennas." In 2019, he was appointed as an Officer of order of Canada "for his fundamental contributions to the fields of electromagnetics and antenna and satellite development, which have led to renowned advancements in the telecommunications industry." In 1986, he established the Symposium on Antenna Technology and Applied Electromagnetics, ANTEM, at the University of Manitoba, which has grown to be the premier Canadian conference in Antenna technology and related topics.